

Article

The Interplay of Processing-Related Influences on the Formation of Volume Holographic Gratings in a Free-Surface Epoxy-Based Recording Material

Tina Sabel-Grau 

Department of Chemistry, Technische Universität Berlin, 10623 Berlin, Germany; tina@physik.tu-berlin.de

Abstract: Understanding the formation processes of holographic gratings in polymers as a function of material composition and processing is important for the development of new materials for holography and its associated applications. Among the processing-related factors that affect grating formation in volume holographic recording material, pre-exposure, prebaking and dark storage, as well as the associated variations in layer thickness and composition, are usually underestimated. This study highlights the influence and interaction of these factors and shows that they should not be neglected. This is of particular importance for samples with a free surface. Here, one such epoxy-based free-surface material is investigated. To determine the influence of prebaking on the holographic grating formation, as well as on the achieved refractive index contrast, angular resolved analysis of volume holographic phase gratings is applied through point-by-point scanning of the local material response. Grating characteristics are determined by comparison with simulations based on rigorous coupled wave theory. Thus, the optimal dose for prebaking can be determined, as well as the optimal exposure time, depending on the dose. The influence of dark storage on the material response is investigated over a period of 12 weeks and shows a strong dependence on the deposited energy density.

Keywords: photosensitive polymers; volume holographic gratings; diffractive optical elements; material response; pre-exposure; layer thickness; dark storage; holographic grating formation; refractive index contrast; polymerization-diffusion-process



Citation: Sabel-Grau, T. The Interplay of Processing-Related Influences on the Formation of Volume Holographic Gratings in a Free-Surface Epoxy-Based Recording Material. *Macromol* **2023**, *3*, 211–223. <https://doi.org/10.3390/macromol3020013>

Academic Editor: Ana María Díez-Pascual

Received: 28 March 2023

Revised: 4 May 2023

Accepted: 5 May 2023

Published: 9 May 2023



Copyright: © 2023 by the author. Licensee MDPI, Basel, Switzerland. This article is an open access article distributed under the terms and conditions of the Creative Commons Attribution (CC BY) license (<https://creativecommons.org/licenses/by/4.0/>).

1. Introduction

Research into new materials for volume holography is being driven by numerous promising applications, from recording media, holographic data storage, self-describing waveguides and wavelength-selective devices [1–3] via holographic sensors based on angular and wavelength selectivity [4] and biosensors [5] to solar energy concentrators, displays and light management [6]. The vast field of lightweight diffractive optical elements that can replace conventional optics is particularly worthy of mention [6]. Here, volume holographic optical elements (vHOE) with the underlying reaction diffusion-driven photopolymerization process play a special role [7]. They can be realized in guest–host systems based on cationic [8] or free-radical [9] ring-opening polymerization, achieving high diffraction efficiency. Here, new application areas are also constantly being added, such as diffractive elements for biomedical applications [10].

New materials for volume holography are constantly being developed and researched more and more intensively [2,11]. New compositions, e.g., focusing on biodegradable components [12] or hydrogels [13], or new photosensitizers based on natural dye [14], are being explored, while increasing the sensitivity and diffraction efficiency of the recorded gratings. The key to exploring and optimizing volume holographic materials for various applications is their design and understanding of the underlying grating formation processes [15]. Regardless of the particular grating formation mechanism—whether it is

based on polymerization or on liquid crystals or whatever—understanding the interactions between the mechanism of grating formation and the underlying molecular processes helps optimize device performance for novel optical systems [16,17].

Photosensitive polymers represent a particularly interesting group among stimulus-responsive polymeric materials for volume holography, characterized by their ability to be applied in a non-invasive and easily controllable manner [18] with no need for solvents while maintaining good dimensional stability and variable thickness. Light as a stimulus means optical patterning by applying volume holography as a one-step method for fabricating diffractive 3D micro- and nanostructures [19].

The mechanisms underlying the formation of volume holographic gratings in polymeric materials can be described by the polymerization–diffusion process, with the chemical gradient as the driving force [20–23]. Figure 1 illustrates the grating formation mechanism, with 1A representing the material composition based on the guest–host system. Accordingly, the gratings are formed primarily as a result of photopolymerization and mass transfer processes: A light (interference) pattern is projected into the photosensitive medium in the course of exposure (Figure 1B), triggering local polymerization, which is proportional to the light intensity. This, in turn, induces a chemical gradient, followed by diffusion of monomers, which in turn also polymerize (Figure 1C). The final grating forms as a periodic modulation of the optical properties in accordance with the recorded light pattern [1].

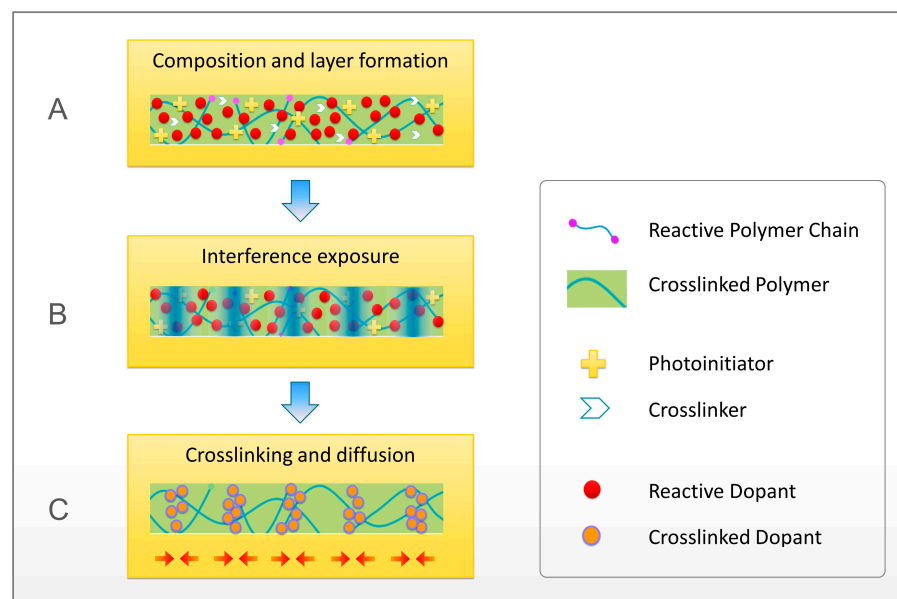


Figure 1. Schematic illustration of grating formation in the guest–host polymer: (A) Composition and layer formation based on the polymer host with reactive chains, dopant, photoinitiator and crosslinker. (B) Interference exposure induces local polymerization, which leads to (C) crosslinking and diffusion, resulting in the final grating.

In developing and optimizing new materials for volume holography, the determination of the material response to processing and exposure conditions is of paramount importance [24]. Here, the criteria for performance evaluation are high energetic sensitivity, wide dynamic range and sharp angular selectivity [25,26]. From the study of the light-induced material response, information about the mechanism of volume hologram formation can be obtained [27]. With insufficient knowledge of the influence of external factors, it is not possible to accurately determine the material response when studying diffraction properties. In other words, without knowledge of the effects of each factor, it is not possible to distinguish whether the change in material composition or processing, on

the one hand, or the exposure or pre-exposure conditions, on the other, affects the response of the material [24].

Most often, the response of the material to the energy density of the exposure—the product of exposure intensity and exposure duration—is studied and well understood [7], while other influencing factors, such as pre-exposure or storage of the samples in the dark, are still too little examined [28]. However, these always play a role—for our example, as soon as more than one hologram is produced per sample and as soon as more than a few days elapse between preparation and exposure of the photosensitive samples. Strictly speaking, on the one hand, the pre-exposure level accumulates by scattered light from grating to grating and on the other hand, the storage of the samples—especially those with a free surface—can have an influence on the diffusion speed via the material viscosity.

Processing-related factors, which are usually underestimated, influence grating formation in volume holographic recording material, including pre-exposure, prebaking, dark storage and related variations in film thickness and composition, while the individual factors can also influence each other [29]. For example, a curing process may allow stabilization of the hologram, but at the same time may lead to a decrease in diffraction efficiency [30].

It is an exciting task to explore the mutual influence of material composition and processing, exposure and pre-exposure on grating formation in volume holographic materials. Based on the study of the material response, diffusion models can be built to predict the behavior of the materials [23,31].

The influence of pre-exposure has already been studied in detail, both on the formation of holograms in real time and on their final, permanent diffraction characteristics [24]. Here, it has already been shown that pre-exposure, e.g., by pre-recorded holograms, should not be underestimated.

The influence of the prebake on the temporal evolution of the grating formation has been studied, and it has been shown that grating growth strongly depends on the prebake duration [26]. It also affects the dependence on exposure duration.

In addition, with other photosensitive materials for volume holography, it has recently been demonstrated that the achievable refractive index contrast can be improved by thermal post-processing techniques [6].

The present study examines the influence of prebaking and dark storage, as well as pre-exposure of photosensitive samples, together with the associated variations in layer thickness and composition. For this purpose, in addition to time-resolved studies, angle-resolved investigations are used, which are completed through point-by-point scanning of the local material response [32].

2. Materials and Methods

2.1. Sample Preparation and Pre-Exposure Treatment

2.1.1. Guest–Host System

Free surface, ultraviolet curable epoxy-based samples were prepared by micro resist technology GmbH (Berlin, Germany). Both host and guest molecules featured epoxy functional groups (Figure 2A), with the corresponding mechanism of cationic ring-opening polymerization. The refractive indices of the host and guest components at 589 nm were $n_{\text{host}} \approx 1.58$ and $n_{\text{guest}} \approx 1.46$, respectively.

2.1.2. Sensitization

A sensitized photoacid generator (PAG) was used to induce crosslinking by cationic polymerization at 405 nm [8]. A strong protonic acid was used to sensitize the mixture. Polymerization was initiated via the initial formation of free radicals. The photoinitiator system consisted of a photosensitive dye, proton donor and onium salt. The proton donor for cationic photopolymerization was formed by photolysis of triaryl sulfonium salt (see Figure 2B).

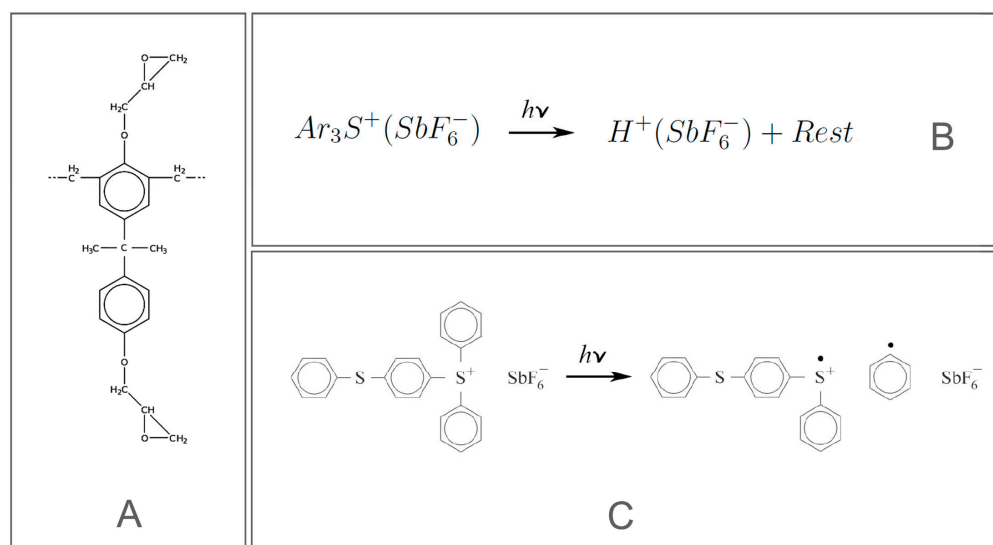


Figure 2. Chemical structure and mechanisms of the guest–host system. (A) A single SU-8 unit with epoxy functional groups. (B) The proton donor for cationic photopolymerization is formed by photolysis of triaryl sulfonium salt. (C) Triarylsulfonium hexafluoroantimonate (TASHFA) undergoes photodecomposition under UV light.

Exposed to UV light, the triarylsulfonium hexafluoroantimonate (TASHFA) underwent photodecomposition (see Figure 2C). Free radicals were produced by subsequently extracting hydrogen ions from the proton donor. As a consequence, the cross-linking of the resin was initiated [33]. As long as consecutive exposures did not entirely consume all of the TASHFA, the mixture remained light sensitive. This is particularly important with respect to multiplexing techniques [34] and for the evaluation of pre-exposure influence. Furthermore, if the TASHFA is not fully decomposed during the curing process, the residual photoinitiator may be available to initiate surface grafting upon further exposure to UV light [33]. Most cationic ring-opening polymerizations involve the formation and propagation of oxonium ion centers. The reaction involves the nucleophilic attack of monomer on the oxonium ion [35].

2.1.3. Crosslinking and Glass Transition Temperature

The epoxy functional groups undergo molecular crosslinking. The corresponding mechanism of polymerization is cationic ring-opening polymerization (CROP): The epoxy functional group reacts with the proton, provided as a result of the exposure by the photoinitiator system, as described above. During the initiation process, the proton attacks the oxygen atom of the epoxy group. The activated monomer reacts with a second monomer in terms of a ring-opening mechanism. During the propagation of the chain reaction, the reactive chain end persists in the form of a tertiary oxonium ion.

As the reaction proceeds and the molecular weight of the epoxy network increases, the viscosity of the material starts to increase, resulting in gelation, vitrification and the formation of highly crosslinked solid epoxy [36]. The glass transition temperature of the evolving network increases and the activation energy decreases.

The glass transition temperature T_G of the host–guest system plays an essential role with respect to the flexibility of the matrix, determining the diffusion ability during grating formation, on the one hand and the stability of the final structure, on the other hand. The upper and lower limits of T_G , depending on the degree of curing, are therefore most important for the applicability of the material as a holographic storage system [37].

We identified the glass transition temperature of the composition to be $T_G = 25$ °C. This ensures sufficient mobility for monomer diffusion, while crosslinking reduces the mobility of the matrix. Fixation by UV flood exposure (dose 350 mJ/cm²) and hard bake up to 140 °C results in $T_G = 130$ °C [8].

2.1.4. Spinning and Prebake

The layers were prepared by spin coating the material in a solution on circular glass substrates of 1 mm thickness. The layer thickness depended on the rotation speed (see Figure 3). A rotation speed of 800 min^{-1} results in a layer thickness of $200 \mu\text{m}$.

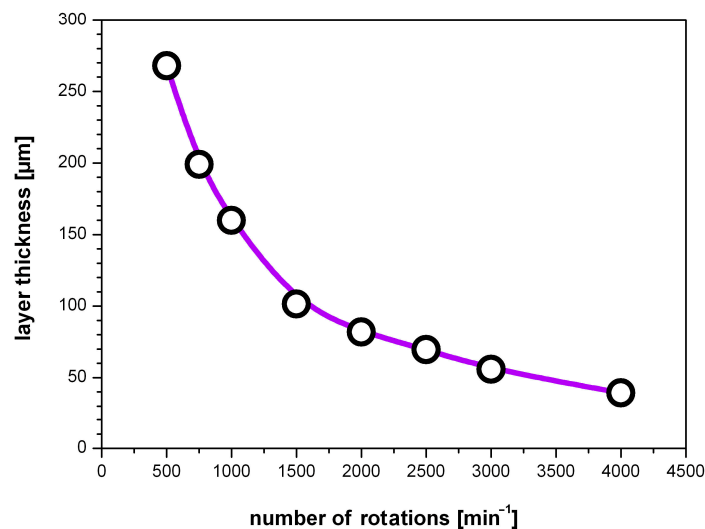


Figure 3. Correlation between the thickness of the photosensitive layer and the number of rotations during sample preparation by means of spin coating.

A subsequent pre-exposure bake was carried out on a hotplate ($80 \text{ }^\circ\text{C}$) for 0.5 to 3 h to drive out the remaining solvent in order to obtain a tack-free film. Long baking times were necessary for good process control in the case of ultra-thick ($>200 \mu\text{m}$) layers [38]. More details on the host-guest system in terms of composition, as well as performance (such as energetic sensitivity and angular selectivity) can be found in [8].

2.2. Holographic Exposure and Post-Processing Treatment

All investigations were based on one-dimensional, plane-wave, transmission-type volume holographic gratings. Symmetric recording geometry was applied to create non-slanted gratings [1] with a periodicity of $\Lambda = (2.8 \pm 0.5) \mu\text{m}$. Holographic exposure was performed by two freely propagating, s-polarized recording beams with a wavelength of $\lambda_{\text{exp}} = 405 \text{ nm}$, a beam diameter of 2 mm, and a laser power of $(1.5 \pm 0.5) \text{ mW}$ per beam. The exposure duration t_{exp} varied between 2 s and 15 s. The exposure setup is shown in Figure 4A. Several holograms were recorded per sample, row by row and from left to right within a row. After the completion of the holographic grating formation, samples were fixed by a UV flood cure with a dose of $350 \text{ mJ}/\text{cm}^2$. During this curing step, the remaining photoinitiator is consumed so that the sample is no longer photosensitive. No postbake, hardbake or any other additional development was applied.

2.3. Analysis of Final Holographic Gratings

Angular-resolved analysis and lateral scanning were applied to characterize the final holographic gratings. Angular-resolved investigations allow the determination of Bragg selectivity, which defines the optical functionality. Therefore, a rotation-scan setup (see Figure 4B) with a collimated probe beam was used [1,8]. The transmitted signal of a HeNe laser ($\lambda_p = 543 \text{ nm}$) is detected while the hologram under test is rotated. The diffraction efficiency was calculated from the angular-resolved transmission. By comparing the angular resolved diffraction efficiency with a rigorous solution of the coupled wave

theory (RCWT) [39], the layer thickness d and the refractive index contrast Δn were derived: The diffraction efficiency η for a probe wavelength λ and the probe angle ϑ_p is given by:

$$\eta = \sin^2 \left(\frac{\pi d \Delta n}{2\lambda \cos(\vartheta_p)} \right) \quad (1)$$

The probe beam diameter was 0.2 mm. Probing only a tenth of the exposed area allowed precise determination of the local material response [33].

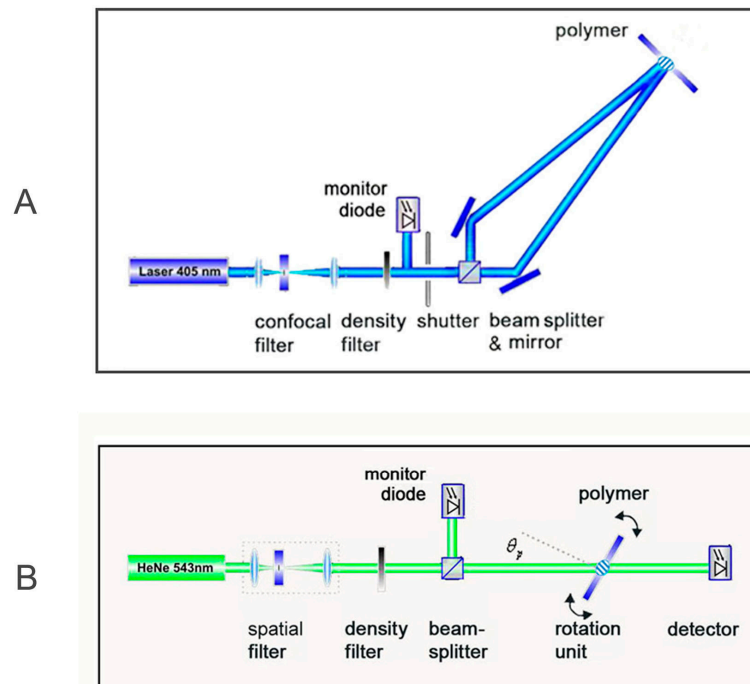


Figure 4. Holographic recording and analysis setups. (A) Holograms are recorded with two freely propagating 405 nm recording beams. (B) Analysis is accomplished with a 543 nm rotation scan setup.

3. Results and Discussion

3.1. Influence of Prebake

Figure 5 shows individual angle-resolved investigations for different prebake durations and exposure times. Figure 5 shows the exact point for point analysis of three holograms with different prebake durations and comparable exposure time. In each case, the prebake duration was 1.5 h (A, B, C), 2 h (D) and 3 h (E, F). The exposure time varied between 2 s and 15 s.

Simulations according to RCWT were adapted to all measurements, and the obtained parameters layer thickness d and refractive index contrast Δn were given. Especially for measurement C (Figure 5, middle left), there are some deviations from the RCW Theory that are worth discussing.

The experimental results showed deviations from coupled wave theory, which were probably caused by the Gaussian intensity distribution of the recording beams in combination with a high value of the normalized coupling constant. Deviations from the RCWT simulations existed first in the form of incomplete zero diffraction between the peaks. This effect can also be observed in the case of very thick films. To explore this effect, a non-constant lattice plane space due to spatial variations of Λ can be considered, which is believed to be responsible for the blurring of the Bragg condition [33], leading to incomplete zero diffraction between the peaks. Similar effects have been observed before [40] and could also be interpreted in this way. Second, the strength of the second diffraction order is less pronounced than expected according to the RCWT. Additionally, the initial arguments

for the Gaussian hologram shape provide a reasonable explanation. The diffraction angle in the case of the second order deviates strongly from the original recording configuration. As a consequence, in this case, a less pronounced region of the grating, i.e., at the edge of the Gaussian profile, is probed, resulting in a lower diffraction efficiency than expected. The main reason for the strength of the effects described here is the rapid increase in the material response to the recording intensity [33].

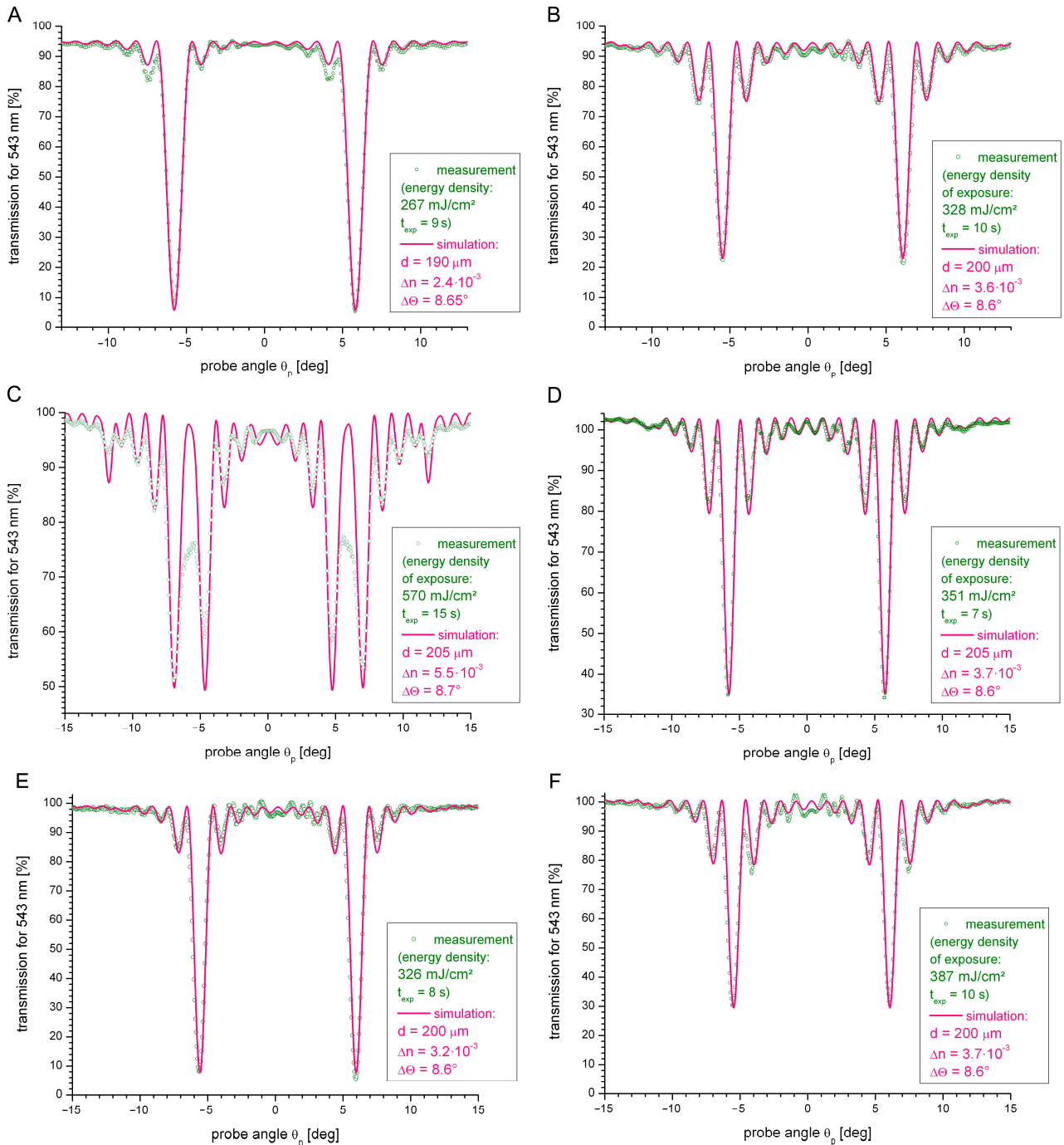


Figure 5. Angular-resolved transmission of samples with prebake durations of 1.5 h (A–C), 2 h (D) and 3 h (E,F). The holograms were recorded with the following exposure times: 9 s (A), 10 s (B), 15 s (C), 7 s (D), 8 s (E) and 10 s (F). Measurements (green circles) are in good agreement with simulations based on rigorous coupled wave theory (pink lines). Layer thickness d and refractive index contrast Δn were determined as important parameters for each hologram.

The main conclusion that can be drawn from the results in Figure 5 is that the investigation of the material response and influence of exposure time depend on the amount of prebake, as shown for samples with a longer prebake duration. The lateral scans reveal an increasingly smaller influence of the exposure time on the material response. The higher the prebake, the greater diffraction efficiencies can be achieved at a constant exposure time.

From Figure 6, it can be seen that the lowest prebake time of 1.5 h provides the best material response in terms of sensitivity, i.e., the greatest diffraction efficiency at low energy density. At the same time, stronger modulated gratings are achieved in the case of a longer prebake for comparable exposure duration: the green curve shows a decrease above 300 mJ/cm^2 , which corresponds to overmodulation (normalized coupling constant $\nu > \pi/2$). The corresponding refractive index contrast is $\Delta n = 3.7 \times 10^{-3}$. The comparison with a rigorous solution of the coupled wave theory (RCWT) can be seen in Figure 5 middle right (D). However, this effect of an improved material response with a longer prebake cannot be continued. The longest prebake duration provides smaller refractive index contrast; here, a normalized coupling constant of $\nu \approx \pi/2$ is just reached.

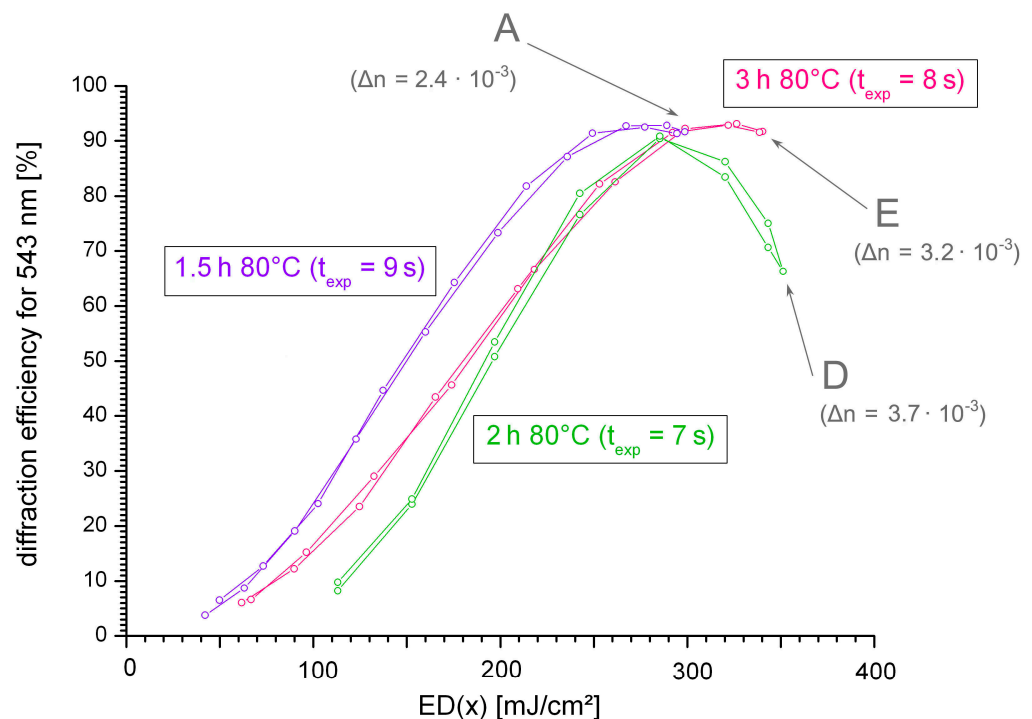


Figure 6. Lateral Scans of samples with different prebake durations and comparable exposure durations. Prebake duration was 1.5 h ($t_{\text{exp}} = 9$ s) for the violet curve, 2 h ($t_{\text{exp}} = 7$ s) for the green curve and 3 h ($t_{\text{exp}} = 8$ s) in case of the pink curve. The individual angle-resolved measurements from Figure 5 are marked (A), (D) and (E) with the corresponding local refractive index contrast Δn .

3.2. Influence of Dark Storage

The special property of a free surface requires consideration of external conditions that may affect its suitability as a holographic recording material. Without a protective layer or the usual sandwich configuration, the photosensitive system is in direct contact with the environment. SU-8 is known to outgas in an unexposed state. The amount of solvent determines the viscosity of the material. Evaporation of the solvent results in a higher viscosity. However, viscosity plays a crucial role in terms of sufficient mobility for monomer diffusion [37].

Interestingly, very long dark storage times can lead to saturation effects with higher harmonics, resulting from high viscosity and consequently slow diffusion rates. By comparison with RCWT simulations, the first-, second- and third-order refractive index contrast can

be derived as described in [8]. For the diffraction curves shown in Figure 5, consideration of the first order $\Delta n^{(0)}$ is sufficient.

Figure 7 shows the influence of dark storage on the material response: diffraction efficiency was investigated over a period of 12 weeks for gratings, differing in deposited energy density. Remarkably, a strong influence of the energy density of exposure can be observed:

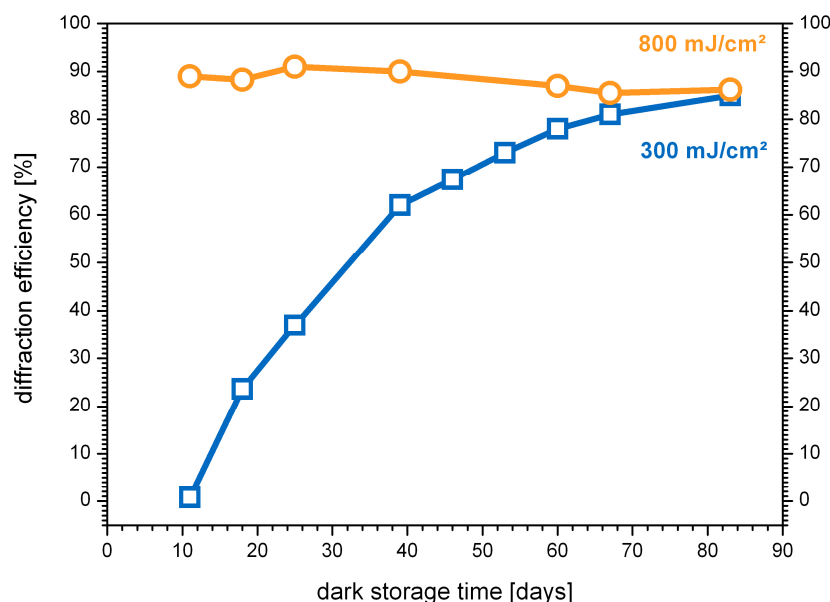


Figure 7. Diffraction efficiency as a function of dark storage time, once for low (300 mJ/cm², blue squares) and once for high (800 mJ/cm², orange circles) energy density.

Gratings recorded with a low exposure dose show a significant increase in diffraction efficiency with increasing storage time. With a high energy density, however, sample storage has no effect on hologram performance. Holograms recorded with high doses show significantly higher diffraction efficiency, exceeding 85%, regardless of the duration of dark storage. However, the low-dose gratings reach the same level after 10 weeks of dark storage.

The constant increasing slope of the curve at a low exposure dose indicates a direct relationship between the viscosity of the material and the performance of the final grating. A destabilizing effect of low viscosity on the gratings may explain the results. Consequently, low viscosity, which is a priori desirable because it facilitates the process of monomer diffusion, seems to have a negative effect on the gratings in the case of a low exposure dose. A blurring of the grating planes in the low viscosity mixture seems reasonable and would lead to weak gratings with low diffraction efficiency. In contrast, a higher dose or longer exposure time could compensate for this instability by increasing the initial crosslinking and stabilizing the grating. This would explain the difference between the low and high dose curves in Figure 7. In contrast, long dark storage times lead to high viscosity and, consequently, slow diffusion rates.

3.3. Impact of Pre-Exposure and Exposure Duration on Layer Thickness

The influence of the pre-exposure of the sample, the position of the hologram on the sample and the exposure time of the hologram is discussed below. These factors are related because several holograms were written per sample, row by row, and within a row from left to right (see right side of Figure 8). Consequently, holograms written subsequently have already experienced pre-exposure by previously written ones, in each case depending on exposure time and duration [25].

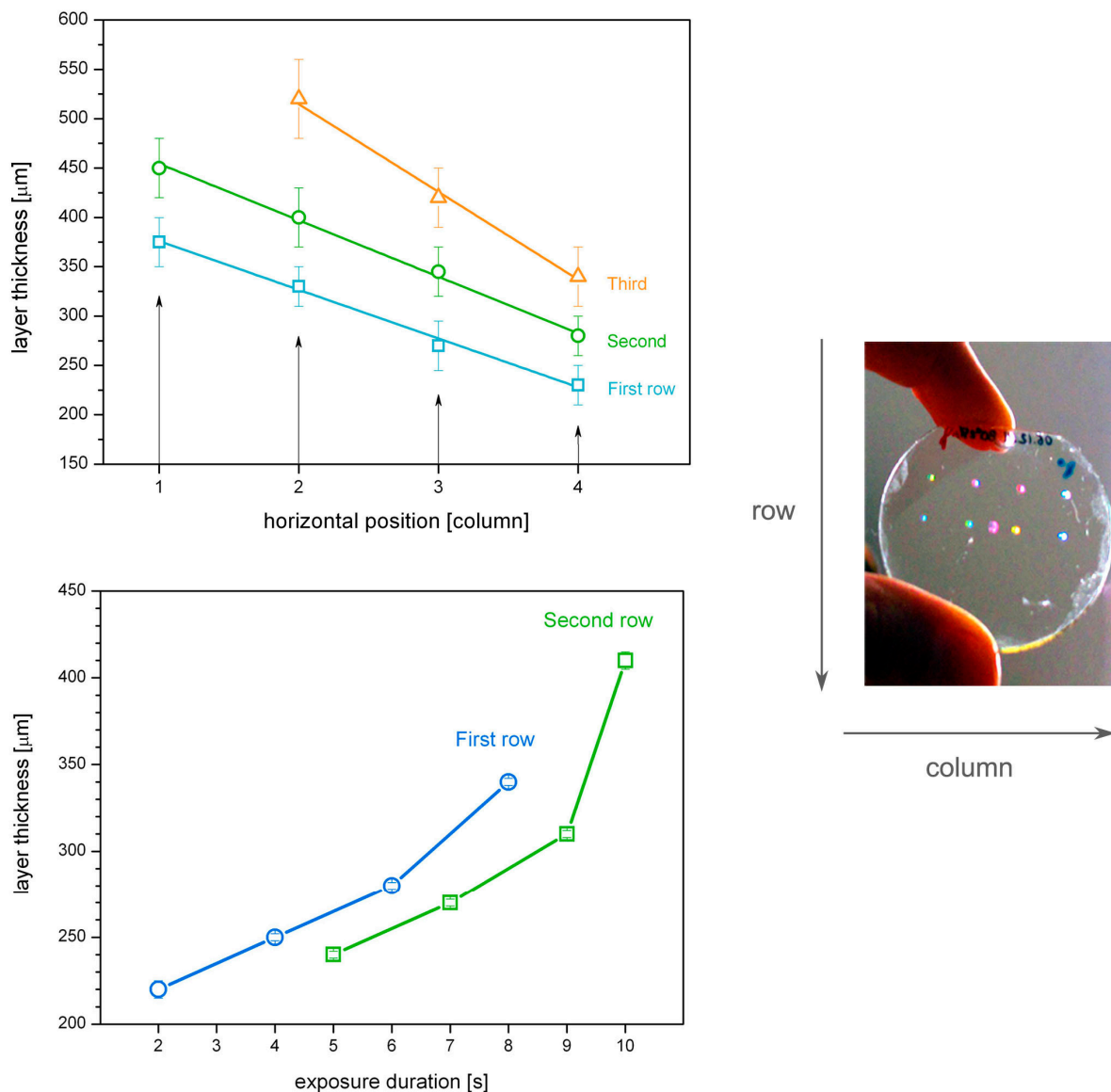


Figure 8. Pre-exposure (**top**) and exposure duration (**bottom**) have an influence on the layer thickness. On the right side, a polymer sample is shown, with indication of the vertical and horizontal position of the holograms in rows and columns.

In general, the interdependency of index modulation and layer thickness, as illustrated in [8], means that within constant index contrast, a variation in layer thickness has a strong impact on the angular response.

Figure 8, left shows that the hologram thickness clearly depends on the position of the sample, which is correlated on the one hand with pre-exposure due to scattering on pre-recorded holograms and on the other hand with a possible flow of the free polymer layer. Shown are the values for the layer thickness derived from RCWT fits via the angular response of the respective holograms. All holograms were generated under constant conditions, i.e., the laser power was constant at 1.5 mW, the exposure time was 15 s in each case, and the exposure geometry results in unslanted gratings with a period of $\Lambda = 2.9 \mu\text{m}$.

Figure 8, left, shows two apparently independent effects. With respect to the horizontal position, the layer thickness decreased with increasing pre-exposure. For the vertical position, the situation is reversed. From row to row, i.e., further down on the vertically positioned sample, thicker gratings are obtained. Although the third row represents a high pre-exposure, possible flowing of the material during dark storage of the samples or

between exposures, which is conceivable, especially with respect to the free and uncovered surface, could be causal for an increase in thickness and cancel the above effect.

In the case of the host–guest system, the issue of material flow is complicated by a possible variation in chemical composition. In this context, a higher guest content could be causal for increased volumetric expansion and thus explain the results shown in Figure 8.

From the findings on the influence of pre-exposure, it can be deduced that the duration of the hologram exposure itself also has an influence on the film thickness. Figure 8 illustrates the interplay of exposure duration and pre-exposure influence on the derived film thickness. The data presented here serve as an example of an overall trend that has been seen several times during the investigations. First, an increase in film thickness with increasing exposure time was evident. However, the opposite effect causes a decrease in film thickness due to a lower vertical position, which is neither consistent with the pre-exposure influence nor with the effect of a possible material flow.

As a possible explanation for the observed swelling phenomenon, volumetric expansion in the course of ring-opening polymerization seems worth considering. Overall, the effect of external influencing factors on hologram thickness d is outlined by the following set of relationships:

$$d \downarrow \leftrightarrow \text{pre-exposure dose}$$

$$d \uparrow \leftrightarrow \text{material flow}$$

$$d \uparrow \leftrightarrow \text{exposure duration.}$$

4. Conclusions

Based on investigations of a novel epoxy-based free surface volume holographic material, the influence of pre-exposure and dark storage on the diffraction characteristics of holograms is studied. Refractive index contrast and film thickness were determined by comparison with RCWT simulations. The influence of processing-related parameters can be explained by the interaction of polymerization and diffusion.

It was found that the lowest prebake time of 1.5 h provided the best material response in terms of sensitivity. At the same time, an effect of improved material response in terms of stronger coupling, i.e., greater refractive index contrast, was observed with longer prebake time. At the longest prebake time, diffusion appeared to be strongly slowed down, resulting in weaker gratings.

The long duration of dark storage seemed to cause a slowdown of polymerization and diffusion. It can be assumed that the diffusion rate D decreases with prebake duration and the reaction rate F decreases with storage time.

In general, the grating growth process depends on the conditions of preparation and exposure. The interplay of polymerization and diffusion is described by parameter R :

$$R = |\mathbf{K}|^2 \frac{D}{F}, \quad (2)$$

with \mathbf{K} being the grating vector, D being the diffusion coefficient and F being half the maximum polymerization rate.

On the one hand, the grating vector \mathbf{K} was adjusted directly via the exposure geometry. The diffusion coefficient D was influenced by the viscosity of the material, which was adjusted by the sample preparation. Actually, viscosity depended on the duration of the prebake procedure. Finally, the polymerization rate F depended on the amount of exposure and thus on the exposure time. Overall, the parameter R and thus grating growth could be controlled by internal and external influencing factors, which could be accessed via preparation and exposure procedures [27].

The so-called diffusion-free condition [41] is associated with a high R parameter, could be caused by sufficient low recording intensity, and corresponded to slow polymerization, fast diffusion and/or small grating periods [27].

Altogether, it could be shown that the influence of pre-exposure due to pre-recorded holograms and the duration of dark storage of samples should not be underestimated but must always be included in the consideration and evaluation of the material response.

Funding: This research was funded by Deutsche Forschungsgemeinschaft (DFG, German Research Foundation), grant number SA 2990/1-1.

Institutional Review Board Statement: Not applicable.

Informed Consent Statement: Not applicable.

Data Availability Statement: The data presented in this study are available on request from the corresponding author.

Acknowledgments: The author thank micro resist technology GmbH for providing the photopolymer material and samples.

Conflicts of Interest: The author declares no conflict of interest. The funders had no role in the design of the study; in the collection, analyses, or interpretation of data; in the writing of the manuscript; or in the decision to publish the results.

References

1. Sabel, T.; Lensen, M.C. Volume Holography: Novel Materials, Methods and Applications. In *Holographic Materials and Optical Systems*; Naydenova, I., Babeva, T., Nazarova, D., Eds.; InTech: Rijeka, Croatia, 2017; pp. 3–25.
2. Guo, J.; Gleeson, M.R.; Sheridan, J.T. A Review of the Optimisation of Photopolymer Materials for Holographic Data Storage. *Phys. Res. Int.* **2012**, *2012*, 803439. [[CrossRef](#)]
3. Malallah, R.; Li, H.; Kelly, D.P.; Healy, J.J.; Sheridan, J.T. A Review of Hologram Storage and Self-Written Waveguides Formation in Photopolymer Media. *Polymers* **2017**, *9*, 337. [[CrossRef](#)] [[PubMed](#)]
4. Mikulchyk, T.; Murphy, K.; Walsh, J.; Martin, S.; Cody, D.; Naydenova, I. Improving the Angular Visibility of Photopolymer-Based Reflection Holograms for Sensing Applications. *Sensors* **2023**, *23*, 4275. [[CrossRef](#)]
5. Zezza, P.; Lucío, M.I.; Fernández, E.; Maquieira, Á.; Bañuls, M.-J. Surface Micro-Patterned Biofunctionalized Hydrogel for Direct Nucleic Acid Hybridization Detection. *Biosensors* **2023**, *13*, 312. [[CrossRef](#)] [[PubMed](#)]
6. Rogers, B.; Mikulchyk, T.; Oubaha, M.; Cody, D.; Martin, S.; Naydenova, I. Improving the Holographic Recording Characteristics of a Water-Resistant Photosensitive Sol-Gel for Use in Volume Holographic Optical Elements. *Photonics* **2022**, *9*, 636. [[CrossRef](#)]
7. Bruder, F.-K.; Fäcke, T.; Rölle, T. The Chemistry and Physics of Bayfol® HX Film Holographic Photopolymer. *Polymers* **2017**, *9*, 472. [[CrossRef](#)] [[PubMed](#)]
8. Sabel, T.; Orlic, S.; Pfeiffer, K.; Ostrzinski, U.; Grütznert, G. Free-surface photopolymerizable recording material for volume holography. *Opt. Mater. Express* **2013**, *3*, 329–338. [[CrossRef](#)]
9. Galli, P.; Evans, R.A.; Bertarelli, C.; Bianco, A. High fidelity holographic recording with cyclic allylic sulfide monomer. *Proc. SPIE* **2020**, *11367*, 123–130.
10. Sabel-Grau, T.; Tyushina, A.; Babalik, C.; Lensen, M.C. UV-VIS Curable PEG Hydrogels for Biomedical Applications with Multifunctionality. *Gels* **2022**, *8*, 164. [[CrossRef](#)]
11. Barachevsky, V.A. The Current Status of the Development of Light-Sensitive Media for Holography (a Review). *Opt. Spectrosc.* **2018**, *124*, 373–407. [[CrossRef](#)]
12. Gumayan, E.G.; Dimzon, I.K.D.; Guerrero, R.A. Chitosan from crab shell waste for soft lithography of bioplastic diffraction gratings. *Appl. Opt.* **2023**, *62*, 2487–2492. [[CrossRef](#)] [[PubMed](#)]
13. Berramdane, K.G.; Ramírez, M.; Zezza, P.; Lucío, M.I.; Bañuls, M.-J.; Maquieira, Á.; Morales-Vidal, M.; Beléndez, A.; Pascual, I. Processing of Holographic Hydrogels in Liquid Media: A Study by High-Performance Liquid Chromatography and Diffraction Efficiency. *Polymers* **2022**, *14*, 2089. [[CrossRef](#)] [[PubMed](#)]
14. Pacheco, K.; Aldea-Nunzi, G.; Pawlicka, A.; Nunzi, J.-M. The Formation of Volume Transmission Gratings in Acrylamide-Based Photopolymers Using Curcumin as a Long-Wavelength Photosensitizer. *Polymers* **2023**, *15*, 1782. [[CrossRef](#)] [[PubMed](#)]
15. Sheridan, J.T.; Kostuk, R.; Fimia, A.; Wang, Y. Roadmap on Holography. *J. Opt.* **2020**, *22*, 65. [[CrossRef](#)]
16. Sabel, T. Volume hologram formation in SU-8 photoresist. *Polymers* **2017**, *9*, 198. [[CrossRef](#)] [[PubMed](#)]
17. Yin, K.; Xiong, J.; He, Z.; Wu, S.-T. Patterning Liquid-Crystal Alignment for Ultrathin Flat Optics. *ACS Omega* **2020**, *5*, 31485–31489. [[CrossRef](#)]
18. Roy, D.; Cambre, J.N.; Sumerlin, B.S. Future perspectives and recent advances in stimuli-responsive materials. *Prog. Polym. Sci.* **2010**, *35*, 278–301. [[CrossRef](#)]
19. Colburn, W.S.; Haines, K.A. Volume Hologram Formation in Photopolymer Materials. *Appl. Opt.* **1971**, *10*, 1636–1641. [[CrossRef](#)]

20. Gallego, S.; Fernández, R.; Márquez, A.; Ortuño, M.; Neipp, C.; Gleeson, M.R.; Sheridan, J.T.; Beléndez, A. Two diffusion photopolymer for sharp diffractive optical elements recording. *Opt. Lett.* **2015**, *40*, 3221–3224. [[CrossRef](#)]
21. Sheridan, J.T.; Downey, M.; Neill, F.O. Diffusion-based model of holographic grating formation in photopolymers: Generalized non-local material responses. *J. Opt. A Pure Appl. Opt.* **2001**, *3*, 477–488. [[CrossRef](#)]
22. Sabel-Grau, T.; Tyushina, A.; Rahman, R.; Babalik, C.; Zhang, Z.; Lensen, M.C. Volume Holographic Structuring of Special Hydrogel Films by Photochemical Crosslinking. In *Holography*; Rosen, J., Ed.; IntechOpen: Rijeka, Croatia, 2022; pp. 199–215.
23. Fernández, R.; Gallego, S.; Márquez, A.; Neipp, C.; Calzado, E.M.; Francés, J.; Morales-Vidal, M.; Beléndez, A. Complex Diffractive Optical Elements Stored in Photopolymers. *Polymers* **2019**, *11*, 1920. [[CrossRef](#)] [[PubMed](#)]
24. Sabel-Grau, T. Influence of Pre-Exposure on the Material Response of Epoxy-Based Volume Holographic Recording Material. *Polymers* **2022**, *14*, 2193. [[CrossRef](#)] [[PubMed](#)]
25. Jeong, Y.-C.; Lee, S.; Park, J.-K. Holographic diffraction gratings with enhanced sensitivity based on epoxy-resin photopolymers. *Opt. Express* **2007**, *15*, 1497–1504. [[CrossRef](#)] [[PubMed](#)]
26. Sabel, T.; Zschocher, M. Transition of refractive index contrast in course of grating growth. *Sci. Rep.* **2013**, *3*, 2552. [[CrossRef](#)]
27. Liu, S.; Gleeson, M.R.; Guo, J.; Sheridan, J.T. High Intensity Response of Photopolymer Materials for Holographic Grating Formation. *Macromolecules* **2010**, *43*, 9462–9472. [[CrossRef](#)]
28. Bruder, F.-K.; Fäcke, T.; Hansen, S.; Manecke, C.; Rewitz, C.; Rölle, T.; Orselli, E.; Wewer, B. On the impact of incoherent pre-exposure on vHOE recording in Bayfol HX film for see-through applications. In *SPIE 10558, Practical Holography XXXII: Displays, Materials, and Applications*; Bjelkhagen, H.I., Bove, V.M., Eds.; SPIE: Bellingham, WA, USA, 2018; p. 18.
29. Sabel, T. Spatial Frequency Response of Epoxy-Based Volume Holographic Recording Material. *Molecules* **2019**, *2*, 1018. [[CrossRef](#)]
30. Morales-Vidal, M.; Ramírez, M.; Sirvent, D.; Martínez Guardiola, F.; Álvarez, M.; Pascual, I. Efficient and stable holographic gratings stored in an environmentally friendly photopolymer. In Proceedings of the IV International Conference on Applications of Optics and Photonics, Lisbon, Portugal, 31 May–4 June 2019; p. 202.
31. Sheridan, J.T.; Lawrence, J.R. Nonlocal-response diffusion model of holographic recording in photopolymer. *J. Opt. Soc. Am. A* **2000**, *17*, 1108–1114. [[CrossRef](#)]
32. Sabel, T. Spatially resolved analysis of Bragg selectivity. *Appl. Sci.* **2015**, *5*, 1064–1075. [[CrossRef](#)]
33. Wang, Y.; Bachman, M.; Sims, C.E.; Li, G.P.; Allbritton, N.L. Simple Photografting Method to Chemically Modify and Micropattern the Surface of SU-8 Photoresist. *Langmuir* **2006**, *22*, 2719–2725. [[CrossRef](#)]
34. Curtis, K.; Psaltis, D. Recording of multiple holograms in photopolymer films. *Appl. Opt.* **1992**, *31*, 7425–7428. [[CrossRef](#)]
35. Odian, G. Ring-Opening Polymerization. In *Principles of Polymerization*; John Wiley & Sons, Ltd.: Hoboken, NJ, USA, 2004; pp. 544–618.
36. Turunen, M.; Laurila, T.; Kivilahti, J. Reactive blending approach to modify spin coated epoxy film: PART II: Crosslinking kinetics. *J. Appl. Polym. Sci.* **2006**, *101*, 3689–3696. [[CrossRef](#)]
37. Ramesh, N.; Duda, J.L. Diffusion in polymers below the glass transition temperature: Comparison of two approaches based on free volume concepts. *Korean J. Chem. Eng.* **2000**, *17*, 310–317. [[CrossRef](#)]
38. Rabarot, M.; Babet, J.; Ruty, M.; Kipp, M.; Chartier, I.; Dubarry, C. Thick SU-8 photolithography for BioMEMS. In *Micromachining and Microfabrication Process Technology VIII*; Yasaitis, J.A., Perez-Maher, M.A., Karam, J.M., Eds.; SPIE: Bellingham, WA, USA, 2003; Volume 4979, pp. 382–393.
39. Moharam, M.G.; Gaylord, T.K. Rigorous coupled-wave analysis of planar-grating diffraction. *J. Opt. Soc. Am.* **1981**, *71*, 811–818. [[CrossRef](#)]
40. Sakhno, O.V.; Goldenberg, L.M.; Smirnova, T.M.; Stumpe, J. Holographic patterning of organic-inorganic photopolymerizable nanocomposites. In *Optical Materials in Defence Systems Technology*; SPIE: Bellingham, WA, USA, 2009; Volume 7487.
41. Piazzolla, S.; Jenkins, B.K. Holographic grating formation in photopolymers. *Opt. Lett.* **1996**, *21*, 1075–1077. [[CrossRef](#)]

Disclaimer/Publisher’s Note: The statements, opinions and data contained in all publications are solely those of the individual author(s) and contributor(s) and not of MDPI and/or the editor(s). MDPI and/or the editor(s) disclaim responsibility for any injury to people or property resulting from any ideas, methods, instructions or products referred to in the content.